Article

Not peer-reviewed version

The Disulfidptosis-Mediated Intercellular Communication in the Tumor Microenvironment Contributes to the Progression of Osteosarcoma and Immunotherapy

Yueying Xiao , Tianze Zhang , Jin Wang , Yanan Wang , Yanqing Huo *

Posted Date: 27 June 2023

doi: 10.20944/preprints202306.1915.v1

Keywords: Disulfidptosis; Osteosarcoma; Tumor immune microenvironment; Immunotherapy; Prognostic model; CAPZB; Intercellular communication

The disulfidptosis-mediated intercellular communication in the tumor microenvironment contributes to the progression of osteosarcoma and immunotherapy

Yueying Xiao[1], Tianze Zhang[2], Jin Wang[3], Yanan Wang[4], Yanqing Huo[1*]

[1] Department of Spine Surgery, The Second Hospital of Shandong University, Shandong University, 250033, Jinan, China.
[2] Department of General Surgery, The Second Hospital, Shandong University, 250033, Jinan, China.
[3] Department of Orthopaedic Trauma, The Second Hospital of Shandong University, Shandong University, 250033, Jinan, China.
[4] Key Laboratory of Experimental Teratology of Ministry of Education, Institute of Medical Sciences, The Second Hospital, Cheeloo College of Medicine, Shandong University, 250033, Jinan, China.
* Correspondence: **Correspondence:** Yanqing Huo; 200462011187@email.sdu.edu.cn

Keywords: Disulfidptosis; Osteosarcoma; Tumor immune microenvironment; Immunotherapy; Prognostic model; CAPZB; Intercellular communication

Abstract: Background: Disulfidptosis, a recently identified form of cell death triggered by excessive cysteine accumulation and subsequent disulfide stress, has emerged as a novel mechanism of cell death. Despite its significance, the role of disulfidptosis in the tumor microenvironment (TME) remains poorly understood. **Methods:** In this study, we employed single-cell RNA sequencing data from 100,987 cells of 11 osteosarcoma (OS) patients. Using the non-negative matrix factorization (NMF) algorithm, we performed dimensionality reduction analysis to identify distinct subtypes characterized by 14 disulfidptosis-related genes across major cell types within the TME. Subsequently, we assessed the prognosis and immunotherapy response associated with each disulfidptosis-related subtype, leveraging publicly available databases comprising osteosarcoma data and immunotherapy cohorts. **Results:** We identified distinct subtypes within tumor-associated fibroblasts, tumor-infiltrating lymphocytes, and macrophages, which we named and annotated based on their characteristic genes. Furthermore, we observed a close association between disulfidptosis-related genes and key biological features of immune cells within the TME, elucidating inferred pseudotime trajectories. Notably, integrating bulk-seq data of osteosarcoma patients, we observed significant differences in overall survival rates among the disulfidptosis-related subtypes. Particularly, the disulfidptosis-related subtype within tumor-associated fibroblasts exhibited superior discriminatory ability in predicting the response of patients undergoing immunotherapy, surpassing other cell subtypes. Our cell-cell communication analysis highlighted extensive and specific interactions between disulfidptosis-related subtypes and osteosarcoma cells. Furthermore, we confirmed the histological localization of the CAPZB+CAF subtype within osteosarcoma tissue and osteoclastoma using immunofluorescence (IF) techniques. **Conclusions:** Collectively, our study sheds light on the intercellular communication facilitated by disulfidptosis in the TME, underscoring its involvement in the biological functions and immunotherapy response of osteosarcoma.

1. Introduction

Osteosarcoma, the most prevalent primary malignant bone tumor, demonstrates a bimodal age distribution with peaks at 18 and 60 years of age, exhibiting a slightly higher incidence in males compared to females[1]. Although surgical interventions, neoadjuvant, and adjuvant chemotherapy have led to significant improvements in patient survival since the 1980s, the prognosis for osteosarcoma remains stagnant[2]. Thus, a comprehensive understanding of the molecular

 doi:10.20944/preprints202306.1915.v1

mechanisms driving osteosarcoma is crucial for developing novel preventive and therapeutic strategies.

Regulated cell death (RCD) refers to a controlled form of cell death that occurs in organisms[3]. Unlike non-regulated forms of cell death, RCD is a highly organized process regulated by multiple signaling pathways and factors. RCD not only plays a vital role in organism development and cellular homeostasis but also contributes to the pathogenesis of various diseases, including cancer[4]. Disulfidptosis is a form of RCD induced by oxidative stress and lipid peroxidation resulting from excessive intracellular free iron (Fe2+)[5]. The uptake of cystine mediated by solute carrier family 7 member 11 (SLC7A11) is pivotal in promoting glutathione synthesis, inhibiting oxidative stress, and regulating ferroptosis. However, recent studies have shown that while SLC7A11-mediated cystine transport can inhibit ferroptosis, it does not prevent cell death under glucose deprivation conditions[6-8]. Additionally, the conversion of cystine imported by SLC7A11 to cysteine heavily relies on the generation of reduced nicotinamide adenine dinucleotide phosphate (NADPH) through the glucose-6-phosphate dehydrogenase (G6PD)-dependent pentose phosphate pathway [9]. Based on this, a recent study revealed a mechanism in which cells expressing high levels of SLC7A11 accumulate abnormal levels of cysteine and other disulfides under glucose-starvation conditions, leading to disulfide stress and rapid cell death. This newly identified form of cell death is termed disulfidptosis[10]. Although research on disulfidptosis is still in its nascent stage, this form of cell death holds promise for developing new avenues for the treatment of osteosarcoma by targeting cancer metabolism.

The tumor microenvironment (TME) plays a crucial role in tumor development and treatment. Investigating the TME provides insights into the mechanisms of tumor progression and offers new strategies for cancer therapy[11]. Advanced techniques for single-cell analysis of cell communication provide valuable information about cell types, subtypes, intercellular interactions, expression and secretion of signaling molecules, as well as spatial and temporal dynamics of communication. These details contribute to our understanding of the mechanisms and regulatory networks underlying cell communication within the TME, laying the foundation for the development of precise therapeutic strategies and immunotherapies[12]. Previous studies have utilized single-cell sequencing technologies to identify major cell types within the TME of osteosarcoma, including osteoblastic osteosarcoma cells, proliferating osteoblastic osteosarcoma cells, chondroblastic osteosarcoma cells, osteoclasts, tumor-infiltrating lymphocytes (TILs, including T cells and NK cells), myeloid cells, fibroblasts, mesenchymal stem cells (MSCs), stromal cells, myocytes, and endothelial cells[13]. These findings establish a foundation for further research. Additionally, metabolic treatments may impact non-tumor cells within the TME, particularly metabolic inhibition of immune cells, which can diminish their anti-tumor efficacy[14]. Similarly, the development of disulfidptosis induction through GLUT inhibition faces challenges in drug development[15]. Therefore, investigating the role of disulfidptosis in the TME may contribute to its clinical translation and the identification of potential immunotherapeutic strategies. However, to date, no study has focused on the interaction between disulfidptosis-related subtypes in the TME and tumor cells.

In this study, we conducted an analysis of 100,987 cells from 11 patients to investigate the impact of disulfidptosis on major immune cells in the TME of osteosarcoma, including fibroblasts, macrophages, and tumor-infiltrating lymphocytes (TILs). We employed Non-negative Matrix Factorization (NMF) to classify the major immune cell populations and define multiple disulfidptosis-related NMF clusters. Fourteen disulfidptosis-related genes were used to delineate the NMF clusters[15]. The results revealed extensive and specific communication between different disulfidptosis-related subtypes in the TME and their significant associations with immune features, immunotherapy response, cellular transcription, and prognosis. To our knowledge, this is the first study to elucidate the communication between osteosarcoma cells and cells in the TME by classifying tumor microenvironment subpopulations using NMF. This study contributes to a better understanding of the underlying mechanisms of osteosarcoma development and advances in immunotherapy.

2. Materials and methods

 doi:10.20944/preprints202306.1915.v1

2.1. Data and clinical sample collection

In this study, we utilized single-cell mRNA sequencing (scRNA-seq) data retrieved from the Gene Expression Omnibus (GEO) database (www.ncbi.nlm.nih.gov) to conduct our analysis. The specific gene set (GSE152048)[13]encompassed RNA sequencing data obtained from 100,987 cells derived from 11 patients diagnosed with osteosarcoma (OS). Among these patients, there were seven cases of primary OS, two cases of recurrent OS, and two cases of pulmonary metastatic OS lesions. Additionally, we acquired mRNA sequence or microarray data, along with clinical information, for an additional 141 osteosarcoma patients from the Therapeutically Applicable Research To Generate Effective Treatments (TARGET) database and the GEO database. In order to carry out immunofluorescence staining, we selected tumor tissue from a patient with osteosarcoma and osteoid tissue from a patient with osteoblastoma, which were subsequently processed into paraffin sections.

2.2. Identification of OS cells and cell types in the TME

The Seurat[16] package in R software (version 4.1.2) was employed to analyze the single-cell RNA sequencing (scRNA-seq) data in this study. We excluded cell samples exhibiting mitochondrial genes accounting for more than 15% of the gene count, as well as those with a minimum gene count of less than 200. Following data normalization using the NormalizeData function, we identified 2000 genes characterized by high intercellular coefficients of variation by utilizing the FindVariableFeatures function within the Seurat package. Subsequently, principal component analysis (PCA) was performed using the ScaleData and RunPCA functions to determine the number of principal components (PCs) based on Seurat objects. For subsequent analysis, we selected 10 PCs and conducted Uniform Manifold Approximation and Projection (UMAP) analysis as well as t-distributed stochastic neighbor embedding (tSNE) analysis. Finally, we employed cell markers obtained from prior experiments to annotate the cell types, thus enabling further analysis.

2.3. Pseudotime trajectory analysis of disulfidptosis-related genes in TME cells

The objective of this study was to examine the relationship between cell developmental trajectories and disulfidptosis-related genes in osteosarcoma. To achieve this, we performed a pseudotime analysis of single-cell RNA data encompassing all cell types present in osteosarcoma. For this purpose, we utilized the "monocle" package[17] and selected highly variable genes based on the following criteria: mean_expression ≥ 0.1 and dispersion_empirical ≥ 1. Subsequently, the plot_pseudotime_heatmap function was applied to the RNA data of various cell types within the immune microenvironment of osteosarcoma. This approach enabled visualization of the expression patterns of disulfidptosis-related genes in the immune microenvironment of osteosarcoma. Through this analysis, our aim was to enhance our understanding of the developmental trajectories of cells in osteosarcoma and their association with the expression of disulfidptosis-related genes.

2.4. Non-negative matrix factorization of disulfidptosis-related genes in TME Cells

In this study, we employed a non-negative matrix factorization (NMF) algorithm[18] to perform dimensionality reduction analysis of disulfidptosis-related genes in different tumor microenvironment (TME) cell types. The NMF algorithm was implemented using the NMF package within the R software. Subsequently, we utilized the results of dimensionality reduction of the expression matrix of disulfidptosis-related genes to identify the distinct isoforms present within these cell types.

2.5. Identification of marker genes of disulfidptosis-related cell subtypes in TME cells

To identify genes that differed between each NMF cluster and all other clusters within each cell type of osteosarcoma tissues, we employed the FindAllMarkers function. We set a logfc.threshold of 0.5 and filtered out genes with a p-value less than 0.05 for subsequent analysis. Each cluster was defined based on the log fold change (logFC) value of the most significantly different gene within that cluster. If the logFC value exceeded 1 and the gene was associated with disulfidptosis, the cluster

 doi:10.20944/preprints202306.1915.v1

was designated as the disulfidptosis-related subtype, and the gene was identified as the marker gene for that cluster. If the logFC value exceeded 1 but the gene was not associated with disulfidptosis, the cluster was classified as the non-disulfidptosis subtype. Similarly, if the logFC value was less than 1 and the gene was not associated with disulfidptosis, the cluster was also classified as the non-disulfidptosis subtype. In cases where the relationship between the gene and disulfidptosis was unclear and the logFC value was less than 1, the cluster was defined as the unclear subtype.

2.6. Cell-cell communication analysis of disulfidptosis-related cell subtypes

To investigate cell-cell communication within disulfidptosis-related cell subtypes, we selected these subtypes and merged them with all osteosarcoma cells. We utilized the cellchat package[19] in R to extract ligand-receptor interaction information from the CellChatDB.human database, enabling the generation of a communication network between each cell subtype. The ComputeCommunProb function was employed to calculate the communication probability/strength between different cell clusters. Subsequently, we visualized the strength of the cell-cell communication network among all cell clusters originating from osteosarcoma cells to other disulfidptosis-related cell clusters using the netVisualCircle function. Finally, we employed the netAnalysis_signalingRole_heatmap function to demonstrate the types and weights of signaling pathways transmitted or received by each cell type.

2.7. SCENIC analysis for disulfidptosis-related subtypes

SCENIC[20] is a powerful tool for analyzing transcription factor activity and gene regulatory networks using single-cell transcriptome data. This analysis consists of three main steps. Initially, the GENIE3 package is utilized to infer the co-expression network of transcription factors (TFs) and genes based on the correlation between TFs and gene expression data from each cell cluster. Subsequently, a gene regulatory network module, known as a regulon, is constructed using the RcisTarget[21] package and two motif databases: hg19-500bp-upstream and hg19-tss-centered. Each regulon contains the TFs and their associated target genes. Finally, the activity of the regulon in each cell is calculated using the AUCell package, and the cumulative curve area (AUC) is determined based on the position of the genes within the regulons in the overall gene expression profile. The AUC value reflects the activity level of the regulon in each individual cell.

2.8. Survival analysis of disulfidptosis-related signatures in public bulk RNA sequence database

We generated different gene expression signatures for disulfidptosis based on the NMF clusters obtained from the FindAllMarkers function. The GSVA function[22] was then utilized to calculate signature scores for each category from the three datasets (TARGET and GEO). Subsequently, we conducted a univariate Cox regression analysis to identify signatures significantly associated with survival. The surv_cutpoint function was employed to determine the optimal cutoff values for these signatures. Finally, based on the optimal cutoff values, we divided the samples into two groups (low and high risk) and plotted Kaplan-Meier survival curves. Survival curves were plotted for the corresponding signature if the p-value was less than 0.05.

2.9. Analysis of immunotherapy in disulfidptosis-related clusters

The TIDE (Tumor Immune Dysfunction and Exclusion)[23] database, an online tool for predicting response to immunotherapy, was utilized for this analysis. We input three gene expression datasets from GEO and TARGET into the TIDE database to obtain immunotherapy response results for patients. Additionally, we obtained clinical activity data of atezolizumab for mUC from a large phase 2 trial (IMvigor210)[24]. The scores of disulfidptosis signatures obtained from the previous GSVA analysis for each database were utilized to identify nmf subtypes associated with immune response.

2.10. Immunofluorescent staining

 doi:10.20944/preprints202306.1915.v1

Immunofluorescent staining of tissue sections was conducted using a TSA fluorescent double staining kit (Servicebio G1235-100T). The primary antibodies used for immunofluorescence included CAPZB (ABclonal A8106) and α-SMA (Servicebio GB13044). The staining procedure commenced with the dewaxing of paraffin sections followed by microwave treatment with citric acid antigen repair solution (pH 6.0) to repair the antigen. Primary and secondary antibodies were added and incubated at room temperature, protected from light. TSA-FITC staining working solution and 5TSA-CY3 staining working solution were used to stain the treated tissue sections. Finally, images were acquired using a multispectral tissue section imaging and analysis system (PerkinElmer Mantra).

2.11. Statistical analysis

To identify variations in immunotherapeutic response and prognosis among disulfidptosis-related cell subtypes, we employed the Wilcoxon rank-sum test. For comparing the biology of disulfidptosis-related cell subtypes within each tumor microenvironment (TME) cell population, we collected multiple sets of genes known to be associated with TME cell function. The AverageExpression function was used to compute the mean expression of each gene in each disulfidptosis-related cell subtype. The pheatmap function was employed to visually represent the expression patterns of the specified genes. Furthermore, we utilized the AddModuleScore[25] function to assign a score to each cell based on CAF isoforms, and the disulfidptosis function was employed to determine the average module scores across different disulfidptosis-related cell subtypes.

3. Results

3.1. Landscape of disulfidptosis-related genes in the tumor microenvironment (TME) of osteosarcoma

The tumor microenvironment (TME) plays a crucial role in the development and progression of osteosarcoma. To understand the landscape of disulfidptosis-related genes within the TME, we analyzed a single-cell RNA sequencing (scRNA-seq) dataset consisting of 71,312 cells from primary osteosarcoma tumors. Based on previous studies[13], we classified the cells in the immune microenvironment into 11 distinct types, including osteoblastic OS cells, proliferating osteoblastic OS cells, chondroblastic OS cells, osteoclastic cells, TILs (T and NK cells), myeloid cells, fibroblasts, pericytes, MSCs, myoblasts, and endothelial cells (Figure 1B).Cell-cell communication analysis using the CellChat package revealed complex communication links between different cell types within the TME (Figure 1C). We examined the distribution of 14 disulfidptosis-related genes in the tSNE clusters using the FeaturePlot function and found that the expression of these genes varied among different TME cell types (Figure 1D). Violin plots were used to visualize the differential expression patterns of key genes (NDUFA11, SLC3A2, NUDFS1) involved in the regulation of cellular redox homeostasis (Figure 1E). Notably, the cysteine transporter protein SLC3A2, which is closely associated with disulfidptosis, was found to be expressed in all TME cells. By utilizing the scRNA data, we classified specific cell types of interest (fibroblasts, macrophages, T cells, and NK cells) into distinct disulfidptosis-related subtypes based on the expression profiles of 14 disulfidptosis-associated genes. The marker genes for these subtypes are listed in supplementary Table 1.

Preprints (www.preprints.org) | NOT PEER-REVIEWED | Posted: 27 June 2023 doi:10.20944/preprints202306.1915.v1

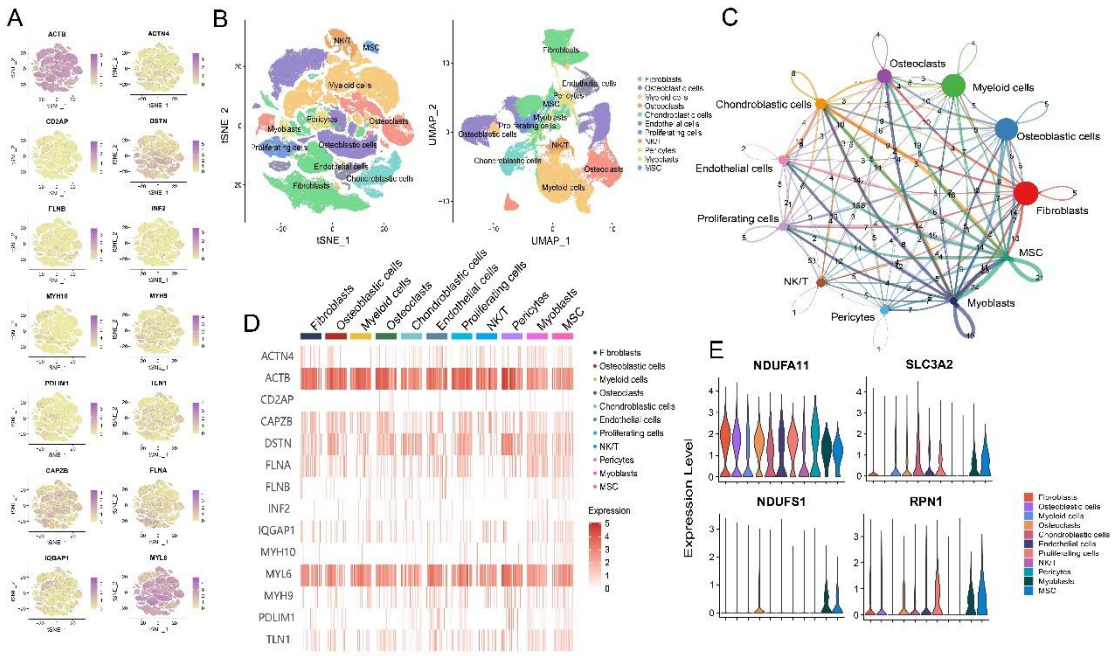

Figure 1. Overview of the study on disulfidptosis-related genes in osteosarcoma single-cell data. (A) Expression of 14 disulfidptosis-related genes depicted on a t-SNE plot. (B) UMAP visualization showing 11 cell types within the single-cell clusters. (C) Cellchat analysis illustrating intercellular communication among the 11 major cell types. (D) Heatmap displaying the distribution of disulfidptosis-related genes in various cell types, including osteoblastic OS cells, proliferating osteoblastic OS cells, chondroblastic OS cells, osteoclastic cells, TILs (T and NK cells), myeloid cells, fibroblasts, pericytes, MSCs, myoblasts, and endothelial cells. (E) Violin plots presenting the expression of four genes closely associated with disulfidptosis regulation.

3.2. Disulfidptosis-driven fibroblasts shape the TME of osteosarcoma

We focused on fibroblasts within the TME and identified 10,447 fibroblasts based on marker genes from a previous study. Using non-negative matrix factorization (NMF), we classified the fibroblast population into 9 subtypes based on 14 disulfidptosis-related genes. Cell-cell communication analysis revealed that these disulfidptosis-related fibroblast subtypes exhibited different interaction patterns with osteosarcoma cells, with ACTN4+CAF-C1 subtype showing the highest number of interactions (Figure 2A, 2B). Pseudotime analysis demonstrated the involvement of disulfidptosis-related genes in the trajectory of fibroblasts (Figure 2D). Scoring the subtypes based on the pan-CAF signature[26] revealed that CAPZB+CAF-C7 correlated significantly with inflammatory CAF (pan-iCAF), while Non-disulfidptosis-CAF-C0 was associated with most tumor-associated fibroblast subtypes (Figure 2C). Furthermore, we examined the outgoing and incoming signals in the fibroblasts and identified the main signals associated with specific subtypes(Figure 2E). The gene regulatory network analysis revealed significant differential expression of transcription factors among the subtypes, with FLNA+CAF-C5 showing upregulation and CAPZB+CAF-C2 showing downregulation(Figure 2F). Additionally, the expression of proinflammatory-related proteins was higher in CAPZB+CAF-C7 (Figure 2G).

Preprints (www.preprints.org) | NOT PEER-REVIEWED | Posted: 27 June 2023 doi:10.20944/preprints202306.1915.v1

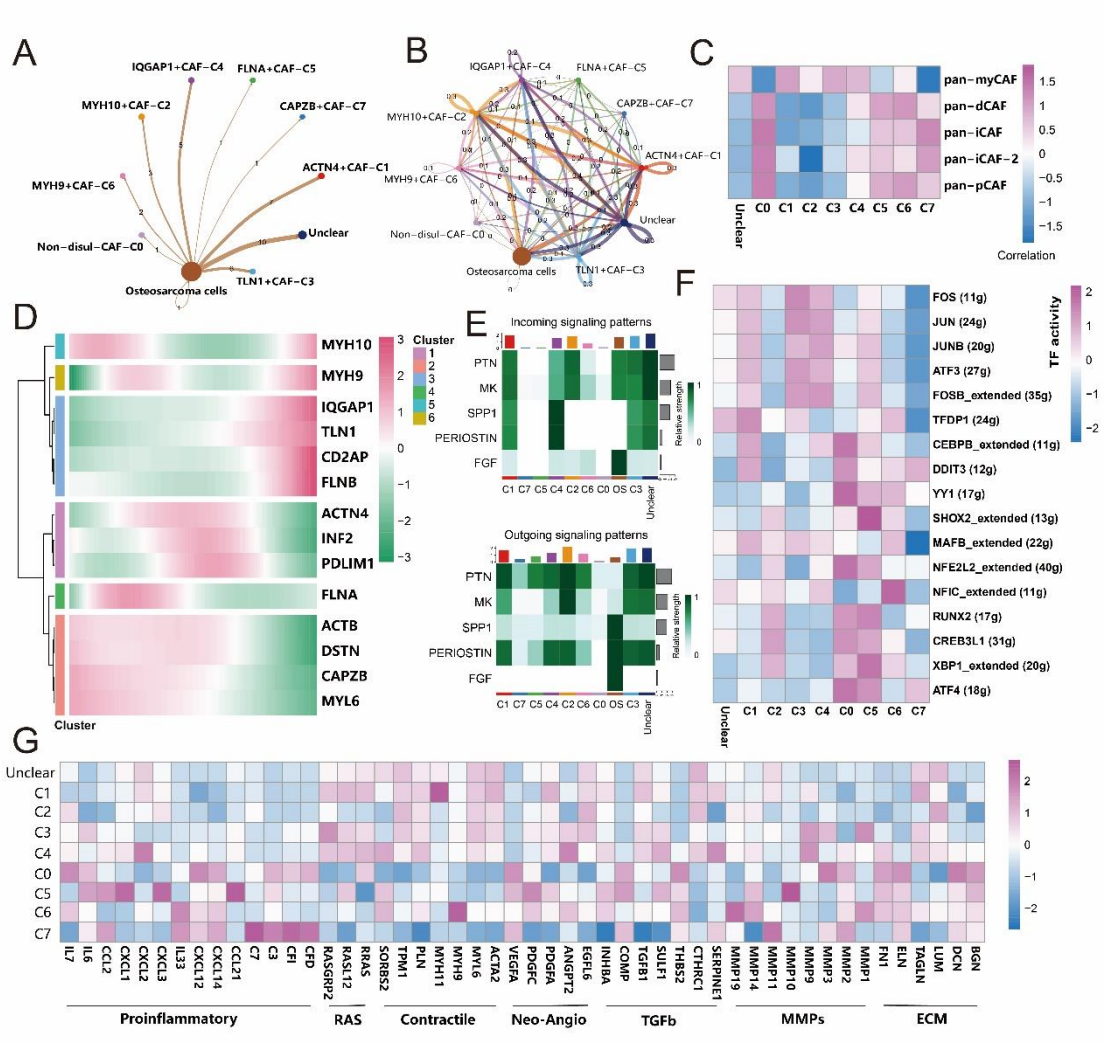

Figure 2. Impact of disulfidptosis on fibroblast characteristics. (A) Cell communication between disulfidptosis-related fibroblast subtypes and osteosarcoma cells. (B) Cell communication between different disulfidptosis-related subtypes, indicating the weightage of each interaction. (C) Association of different disulfidptosis-related subtypes with five pan-CAF subtypes. (D) Pseudotime analysis depicting a clustered heatmap of 14 disulfidptosis-related genes in fibroblasts. (E) Incoming and outgoing signaling patterns of disulfidptosis-related fibroblast subtypes. (F) Comparison of transcription factor activities in seven disulfidptosis-related fibroblast subtypes using the SCENIC package in R. (G) Heatmap displaying the average expression of seven common signaling pathway genes across different disulfidptosis-related fibroblast subtypes.

3.3. Disulfidptosis-driven subtypes of tumor-infiltrating lymphocytes (TILs) impact the immune response in osteosarcoma

Tumor-infiltrating lymphocytes (TILs) play a crucial role in cancer immunotherapy, and their interaction with disulfidptosis remains unclear. Therefore, we categorized TILs in osteosarcoma into eight subtypes, including CD4+ T cells, B cells, CD8+ T cells, NK cells, CD4−/CD8− T cells, proliferating T cells, NKT cells, and T-regulatory cells (Figure 3A). Using the NMF algorithm, we further classified NK cells, CD4+ T cells, CD8+ T cells, and T-regulatory cells into disulfidptosis-related subtypes. The interaction analysis revealed distinct ligand-receptor interactions with osteosarcoma cells for each TIL subtype (Figure 3C). Transcription factor gene regulatory networks showed significant differential expression across disulfidptosis-related subtypes (Figure 3D). We analyzed the expression of co-stimulatory and co-inhibitory markers in different subtypes and observed variations in their average expression levels. Signature scores related to T cell functions, including exhaustion, cytotoxicity, effector function, and effector memory, also differed among the

Preprints (www.preprints.org) | NOT PEER-REVIEWED | Posted: 27 June 2023 doi:10.20944/preprints202306.1915.v1

subtypes(Figure 3B). Pseudotime analysis provided insights into the dynamic characteristics of the NMF-disulfidptosis-related TIL subtypes (Supplementary Figure 1B, 1E; Supplementary Figure 2B, 2E; Supplementary Figure 3B, 3E; Supplementary Figure 4B, 4E). Supplementary Table 2 lists the signature genes for different TIL subtypes. By exploring the landscape of disulfidptosis-related genes in the TME of osteosarcoma, we revealed distinct subtypes of fibroblasts and TILs that contribute to the tumor microenvironment and immune response. These findings enhance our understanding of the role of disulfidptosis in osteosarcoma and provide valuable insights for future research and clinical applications.

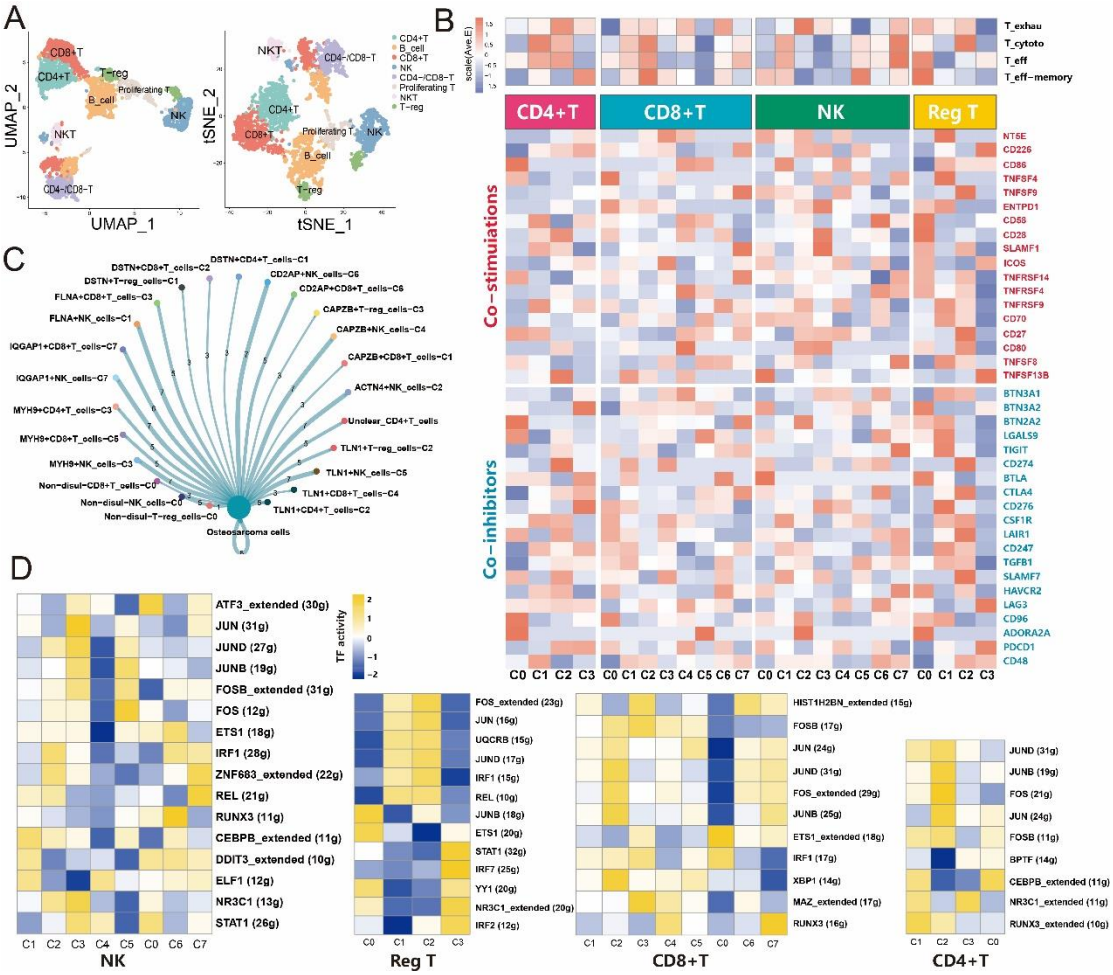

Figure 3. NMF clusters of disulfidptosis-related genes for tumor-infiltrating lymphocytes. (A) UMAP and tSNE maps illustrating the cellular distribution of eight infiltrating lymphocyte subpopulations, including CD4+T cells, B cells, CD8+T cells, natural killer (NK) cells, CD4-/CD8- T cells, proliferating T cells, NKT cells, and regulatory T cells (T-reg). (B) Heatmap displaying different features of NMF clusters, such as four T cell functional scores and the average expression of immune inhibitory and immune activation genes in the four infiltrating lymphocyte subtypes. (C) Cell-cell communication between disulfidptosis-related infiltrating lymphocytes and osteosarcoma cells. (D) Comparison of transcription factor activities in the four infiltrating lymphocyte subtypes using the SCENIC package in R.

Preprints (www.preprints.org) | NOT PEER-REVIEWED | Posted: 27 June 2023 doi:10.20944/preprints202306.1915.v1

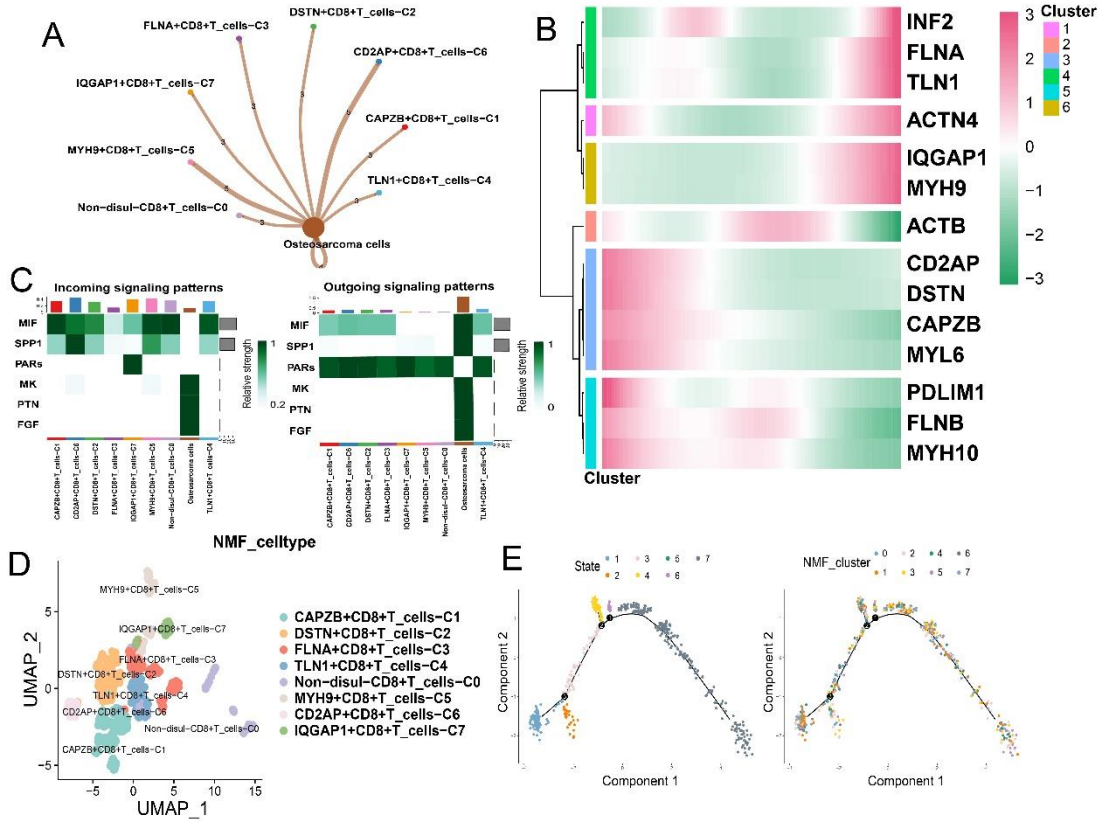

Supplementary Figure 1: Communication analysis and features of disulfidptosis-related subtypes in CD8+ T cells. (A) Cell-cell communication between disulfidptosis-related CD8+ T subtypes and osteosarcoma cells. (B) Pseudotime analysis displaying a clustered heatmap of 14 disulfidptosis-related genes in CD8+ T cells. (C) Incoming and outgoing signaling patterns of disulfidptosis-related CD8+ T subtypes. (D) UMAP plots illustrating different disulfidptosis-related CD8+ T subtypes. (E) Cellular trajectories of different disulfidptosis-related CD8+ T subtypes using monocle.

Preprints (www.preprints.org) | NOT PEER-REVIEWED | Posted: 27 June 2023 doi:10.20944/preprints202306.1915.v1

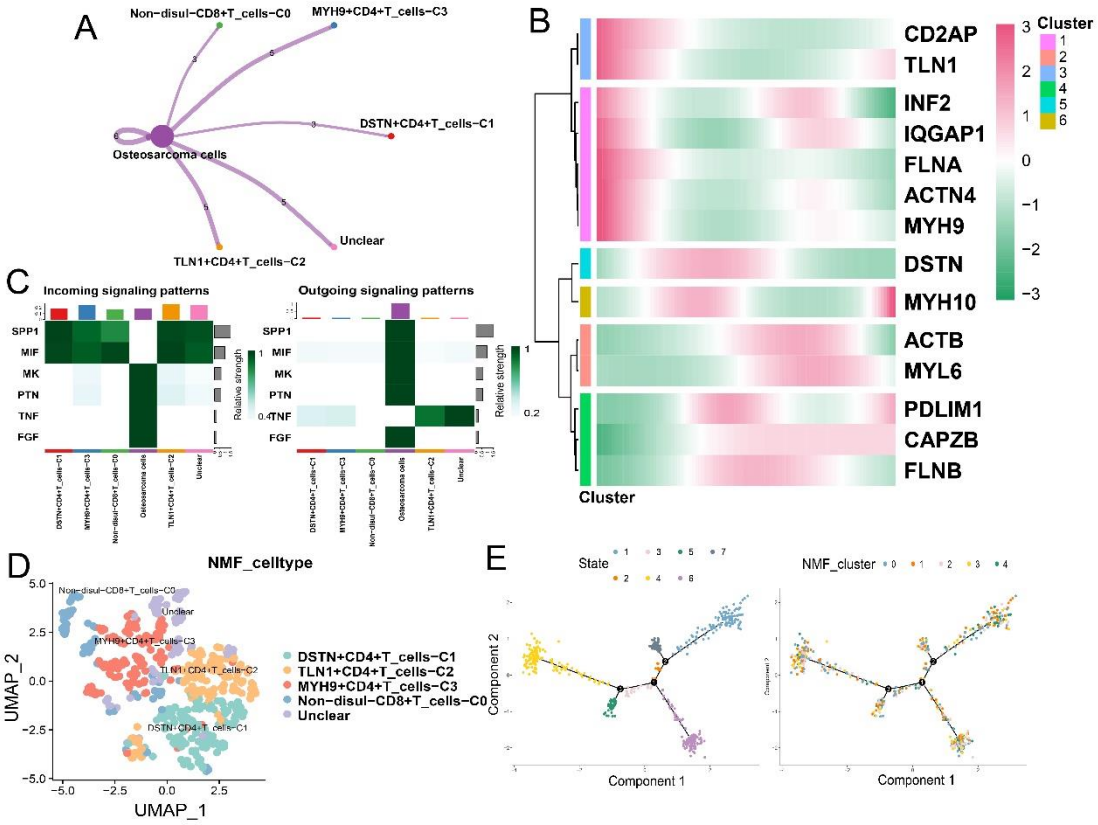

Supplementary Figure 2: Communication analysis and features of disulfidptosis-related subtypes in CD4+ T cells. (A) Cell-cell communication between disulfidptosis-related CD4+ T subtypes and osteosarcoma cells. (B) Pseudotime analysis depicting a clustered heatmap of 14 disulfidptosis-related genes in CD4+ T cells. (C) Incoming and outgoing signaling patterns of disulfidptosis-related CD4+ T subtypes. (D) UMAP plots demonstrating different disulfidptosis-related CD4+ T subtypes. (E) Cellular trajectories of different disulfidptosis-related CD4+ T subtypes using monocle.

Preprints (www.preprints.org) | NOT PEER-REVIEWED | Posted: 27 June 2023 doi:10.20944/preprints202306.1915.v1

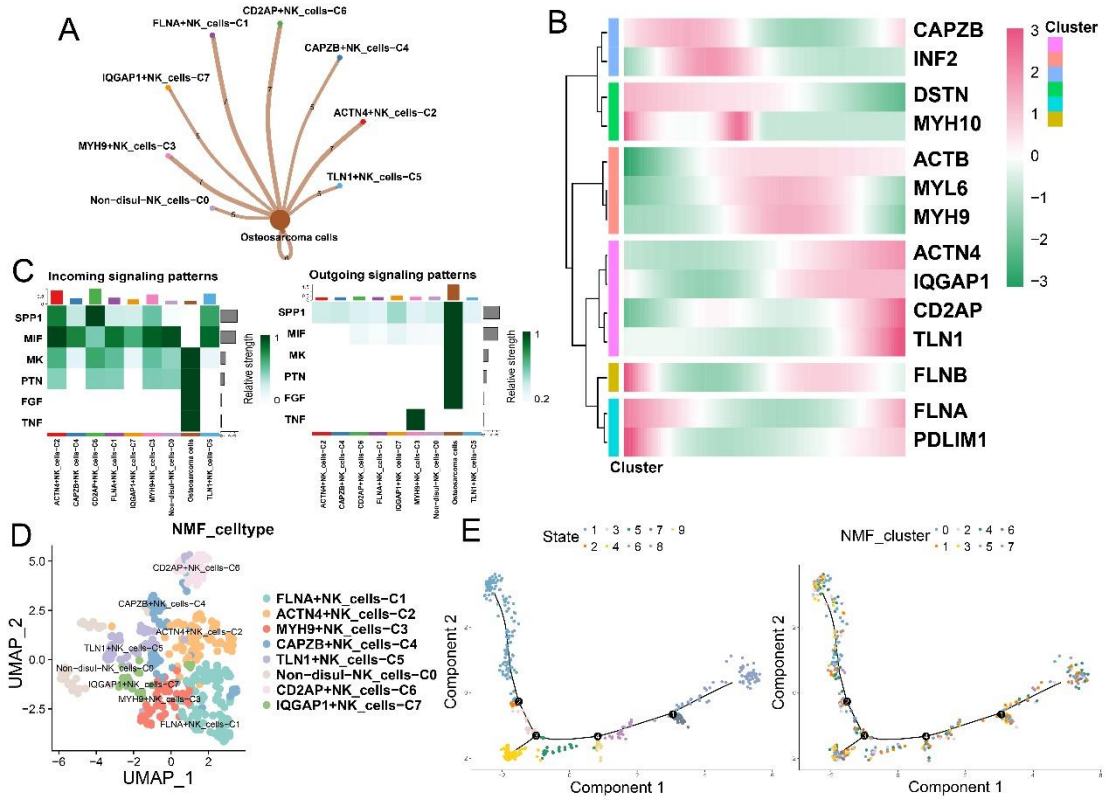

Supplementary Figure 3: Communication analysis and features of disulfidptosis-related subtypes in NK cells. (A) Cell-cell communication between disulfidptosis-related NK cell subtypes and osteosarcoma cells. (B) Pseudotime analysis presenting a clustered heatmap of 14 disulfidptosis-related genes in NK cells. (C) Incoming and outgoing signaling patterns of disulfidptosis-related NK cell subtypes. (D) UMAP plots illustrating different disulfidptosis-related NK cell subtypes. (E) Cellular trajectories of different disulfidptosis-related NK cell subtypes using monocle.

Preprints (www.preprints.org) | NOT PEER-REVIEWED | Posted: 27 June 2023 doi:10.20944/preprints202306.1915.v1

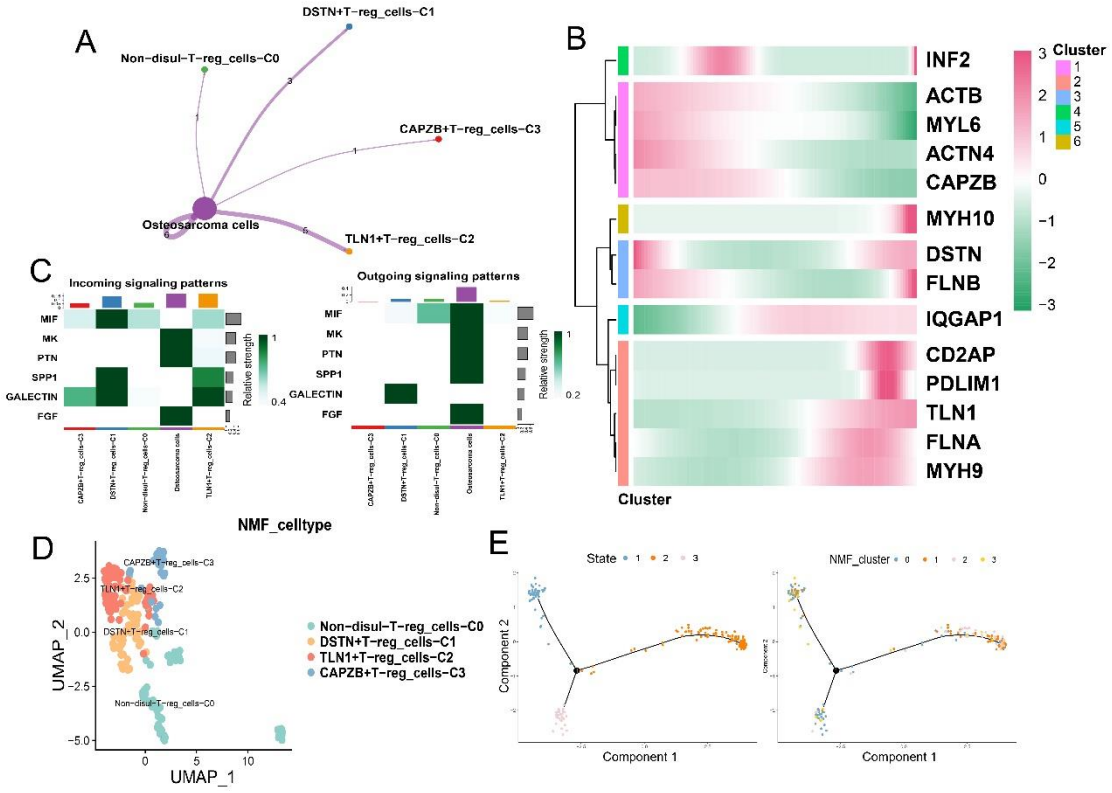

Supplementary Figure 4: Communication analysis and features of disulfidptosis-related subtypes in regulatory T cells. (A) Cell-cell communication between disulfidptosis-related regulatory T cell subtypes and osteosarcoma cells. (B) Pseudotime analysis presenting a clustered heatmap of 14 disulfidptosis-related genes in regulatory T cells. (C) Incoming and outgoing signaling patterns of disulfidptosis-related regulatory T cell subtypes. (D) UMAP plots demonstrating different disulfidptosis-related regulatory T cell subtypes. (E) Cellular trajectories of different disulfidptosis-related regulatory T cell subtypes using monocle.

3.4. Disulfidptosis-driven macrophages: Impact on cellular metabolism and intercellular communication

A total of 24,685 myeloid cells were identified in our analysis. Among them, we selected 3,471 macrophages based on established gene markers from previous literature. Using the NMF algorithm and the expression levels of disulfidptosis-related genes, we classified the macrophages into five major disulfidptosis-related clusters (Figure 4B). These subtypes included three subtypes expressing disulfidptosis genes (INF2+Mac-C2, FLNA+Mac-C3, ACTN4+Mac-C1), one subtype with unclear expression of disulfidptosis genes (Unclear), and one subtype not expressing disulfidptosis genes (Non-disul-Mac-C0). The five disulfidptosis-related subtypes exhibited different numbers of ligand-receptor interactions with osteosarcoma cells (Figure 4A). We visualized the incoming and outgoing signaling propagation networks of cell-cell interactions using heatmap diagrams. Notably, the Non-disul-Mac-C0 subtype showed fewer connections with osteosarcoma cells compared to the other subtypes expressing disulfidptosis-related genes. Additionally, metabolic analysis using the Seurat package revealed distinct differences in the top 30 metabolic pathways among the five subtypes, with the Non-disul-Mac-C0 subtype showing lower pathway scores compared to the other subtypes (Figure 4E). Importantly, there were no significant differences in the distribution and proportions of the five disulfidptosis gene subtypes between M1 and M2 macrophages (Figure 4G, 4F).

Preprints (www.preprints.org) | NOT PEER-REVIEWED | Posted: 27 June 2023 doi:10.20944/preprints202306.1915.v1

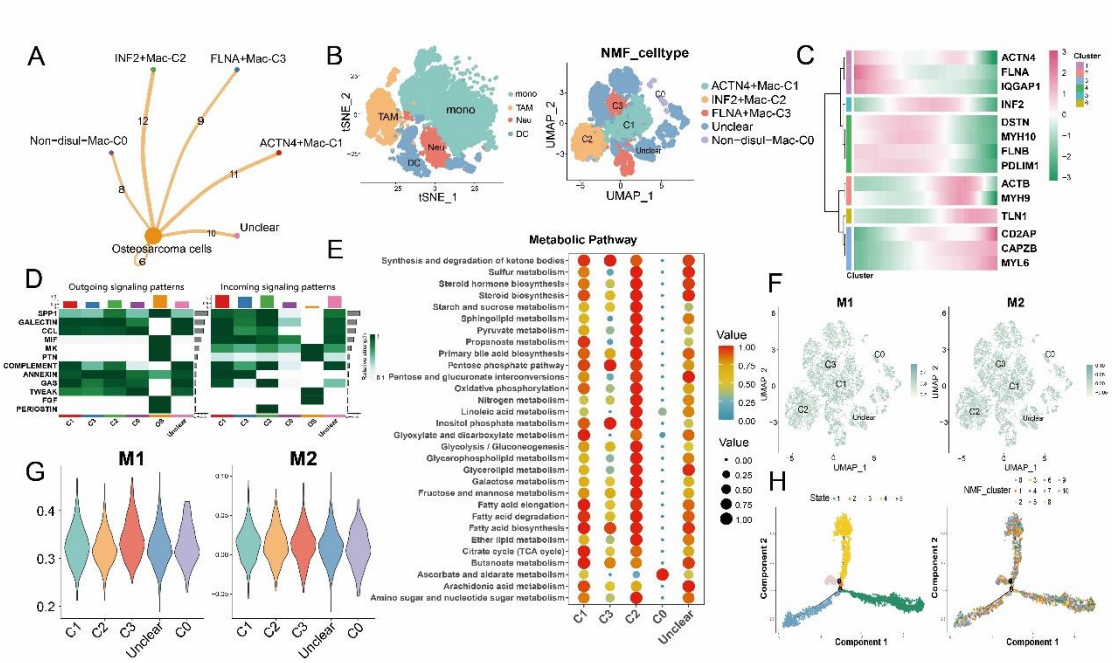

Figure 4. Impact of disulfidptosis on macrophage characteristics. (A) Cell communication between disulfidptosis-related macrophage subtypes and osteosarcoma cells. (B) t-SNE plot of myeloid cells in osteosarcoma TME; UMAP plot of different disulfidptosis-related macrophage subtypes. (C) Pseudotime analysis depicting a clustered heatmap of 14 disulfidptosis-related genes in macrophages. (D) Incoming and outgoing signaling patterns of disulfidptosis-related macrophage subtypes. (E) Heatmap illustrating the scoring differences of four disulfidptosis-related macrophage subtypes across 30 metabolic signaling pathways. (F) UMAP plots of M1 macrophages and M2 macrophages. (G) Differential expression of disulfidptosis-related subtypes in M1 macrophages and M2 macrophages. (H) Cellular trajectories of different disulfidptosis-related subtypes using monocle.

3.5. Impact of disulfidptosis-driven TME on osteosarcoma prognosis

To investigate the relationship between disulfidptosis-related subtypes and prognosis in osteosarcoma, we merged three datasets of prognosis data and corresponding subtype signature scores. This allowed us to establish the correlation between signature scores and survival time. Using a univariate Cox proportional hazards regression model with the survival time and signature scores of 172 patients from the three datasets, we observed significant differences in overall survival among disulfidptosis-related subtypes, which involve alterations in key genes associated with tumor-associated fibroblasts, tumor-infiltrating lymphocytes, and macrophages (Figure 5A). Additionally, based on the disulfidptosis-related signatures of each cell type, we divided patients into high and low expression groups for each gene set and calculated the intergroup differences accordingly. We identified significant differences (p-value < 0.05) in the survival outcomes of four subgroups: CAPZB+NK-C4, CD2AP+NK-C6, MYH9+NK-C3, and MYH10+CAF-C2 across all three gene sets (Supplementary Figure 5).

Preprints (www.preprints.org) | NOT PEER-REVIEWED | Posted: 27 June 2023 doi:10.20944/preprints202306.1915.v1

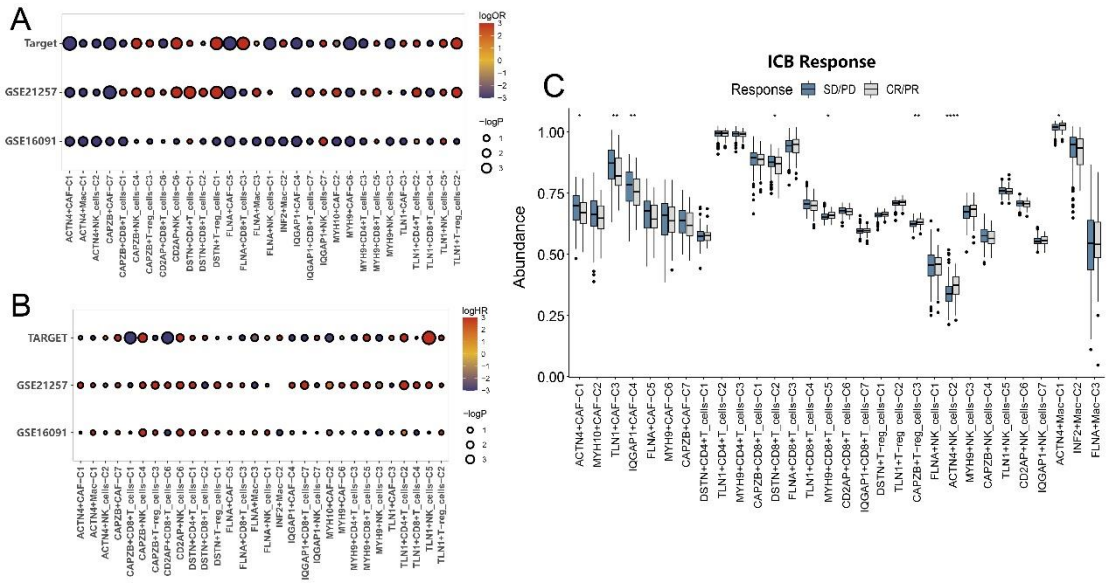

Figure 5. Prognosis and immunotherapy response of disulfidptosis-related subtypes (GSVA scores) in different public cohorts. (A) Analysis of immunotherapy response. (B) Prognosis analysis. (C) Immunotherapy response in a public cohort.

Preprints (www.preprints.org) | NOT PEER-REVIEWED | Posted: 27 June 2023 doi:10.20944/preprints202306.1915.v1

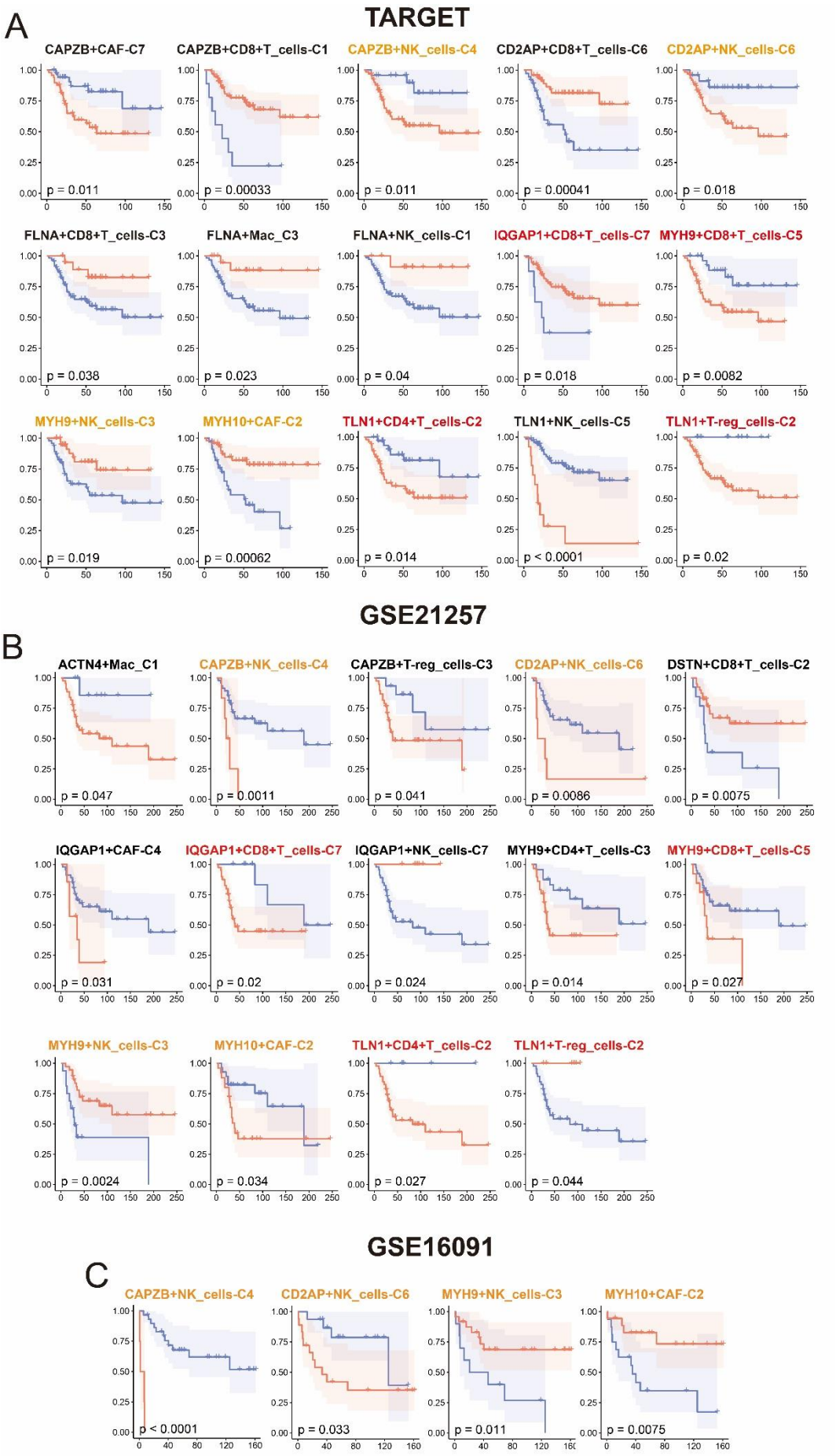

Preprints (www.preprints.org) | NOT PEER-REVIEWED | Posted: 27 June 2023 doi:10.20944/preprints202306.1915.v1

Supplementary Figure 5: Prognosis of disulfidptosis-related subtypes (GSVA scores) in different public cohorts.

3.6. Impact of disulfidptosis-driven TME on immunotherapy in osteosarcoma

Furthermore, we integrated the immunotherapy response results obtained from the TIDE database with the GSVA analysis results. Using the logistic regression method, we consistently observed meaningful associations between the disulfidptosis-related subtypes and immunotherapy response across three osteosarcoma cohorts receiving immunotherapy (Figure 5A). Additionally, we validated the relationship between different disulfidptosis-related TME subtypes and immunotherapy using a cohort dataset of immune therapy for bladder urothelial carcinoma (BLCA) (Figure 5C) (Supplementary Figure 6).

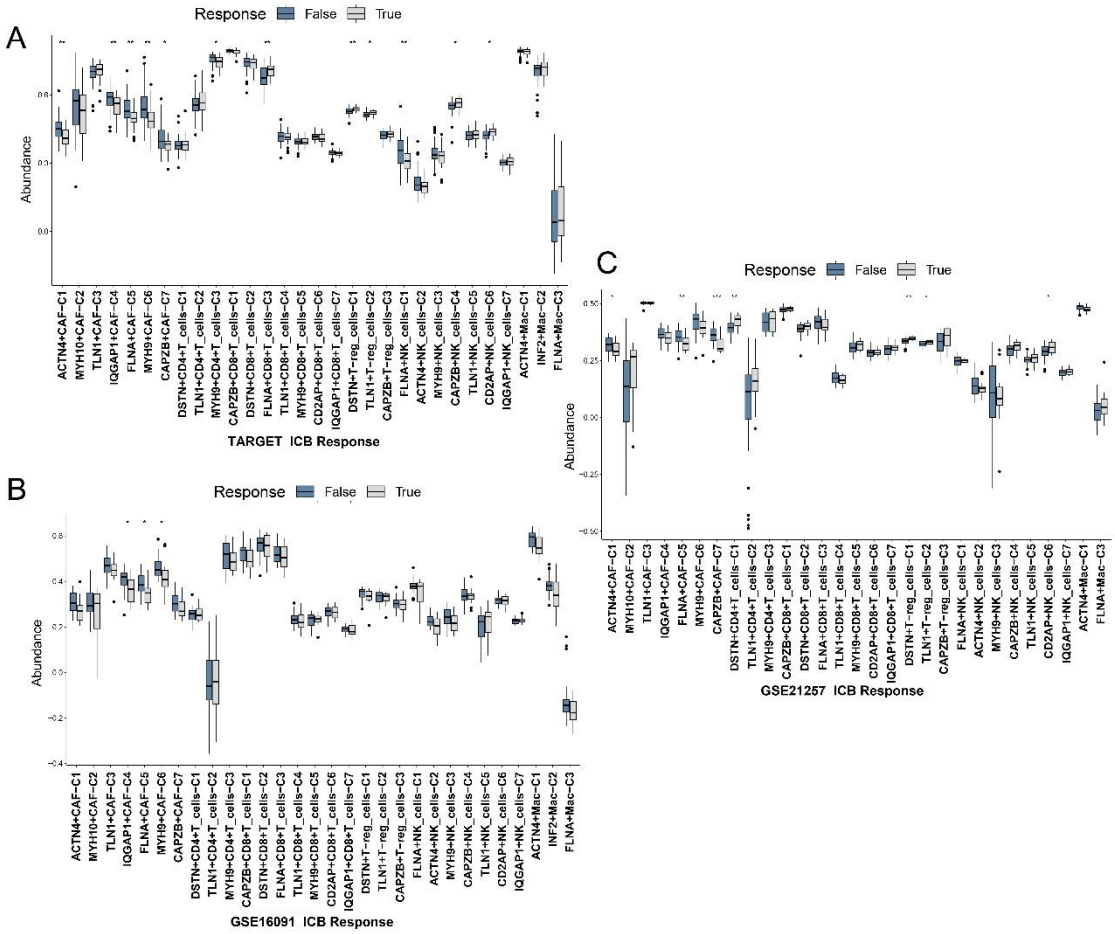

Supplementary Figure 6: Immunotherapy response of disulfidptosis-related subtypes (GSVA scores) in different public cohorts.

3.7. Enhanced intercellular communication in disulfidptosis-mediated TME patterns

Through cell chat analysis of tumor-associated fibroblasts, CD8+ T cells, and macrophages, we identified several ligand-receptor pairs involved in intercellular communication from tumor cells to disulfidptosis-related TME subtypes (Figure 6A)(Supplementary Figure 7). The binding strength and ligand-receptor profiles between disulfidptosis-related TME subtypes and osteosarcoma cells varied, suggesting that these subtypes may engage in extensive interactions with tumor cells, thereby promoting osteosarcoma development (Figure 6B).

Preprints (www.preprints.org) | NOT PEER-REVIEWED | Posted: 27 June 2023 doi:10.20944/preprints202306.1915.v1

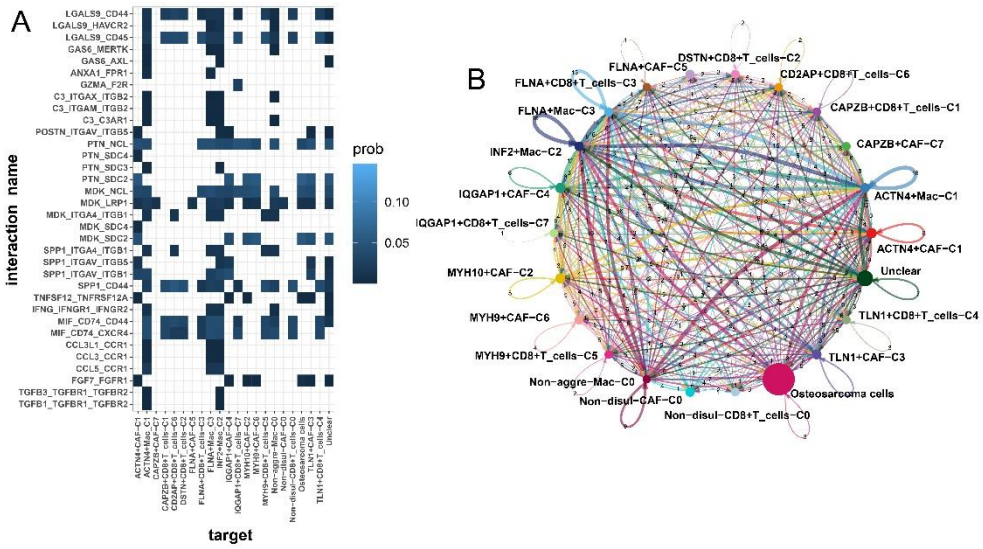

Figure 6. Intercellular communication between major disulfidptosis-related subtypes. (A) Ligand-receptor interactions between major disulfidptosis-related subtypes and osteosarcoma. (B) Cellchat analysis demonstrating cell-cell communication among disulfidptosis-related subtypes.

Preprints (www.preprints.org) | NOT PEER-REVIEWED | Posted: 27 June 2023 doi:10.20944/preprints202306.1915.v1

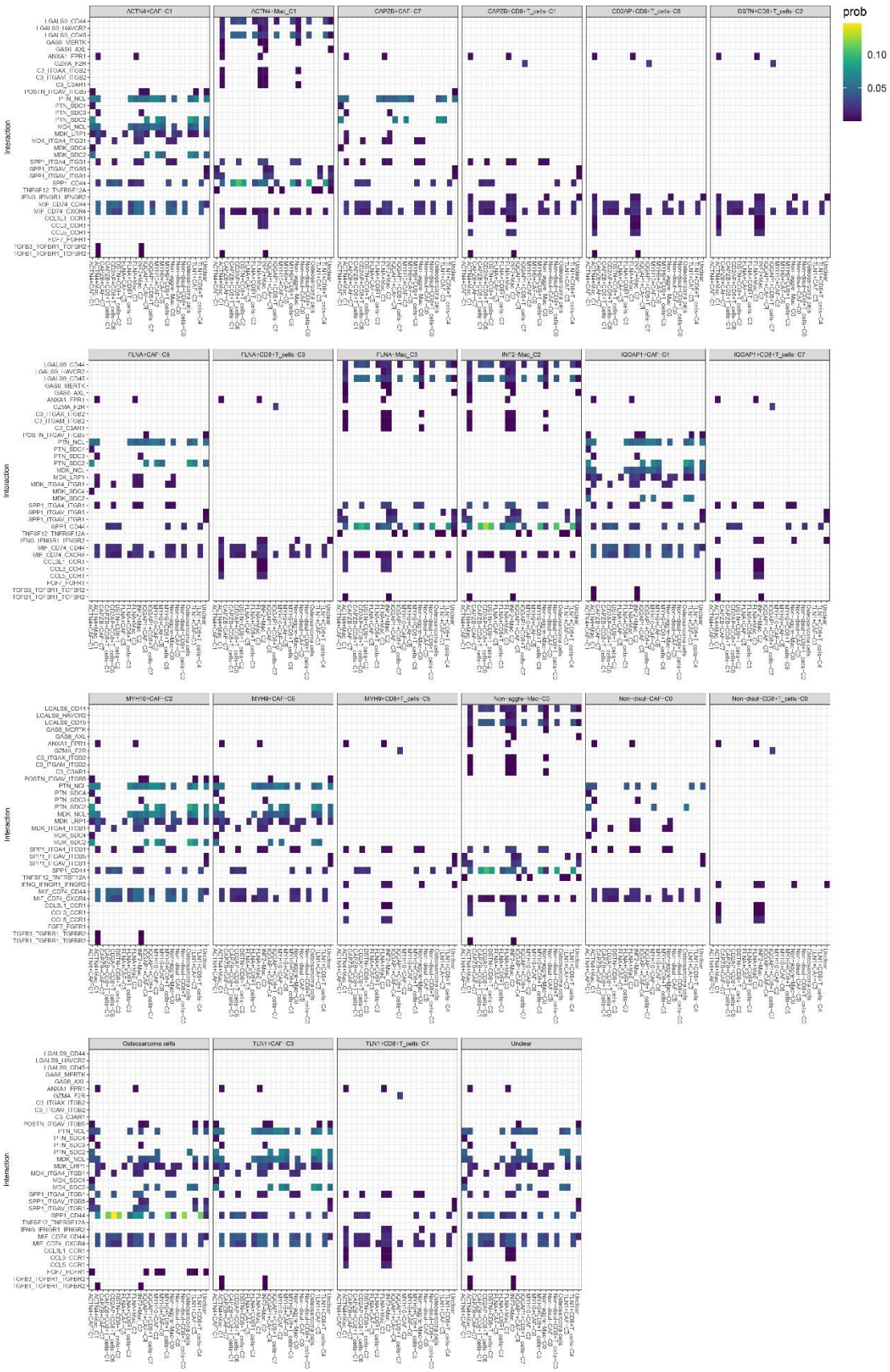

Supplementary Figure 7: Ligand-receptor interactions between all disulfidptosis-related subtypes and osteosarcoma cells.

3.8. Histological localization of CAPZB-CAF-C7 in osteosarcoma and osteoblastoma

Preprints (www.preprints.org) | NOT PEER-REVIEWED | Posted: 27 June 2023 doi:10.20944/preprints202306.1915.v1

We found that CAPZB+CAF-C7, as a subtype of cancer-associated fibroblasts, significantly impacted immunotherapeutic response and overall survival in osteosarcoma(Figure 7). To validate the histological localization of CAPZB+CAF-C7 in osteosarcoma tissues and other benign conditions, we performed immunofluorescence (IF) staining on human osteosarcoma and osteoblastoma tissues. The results revealed a co-localization of the fluorescence signals between α-SMA, a marker for tumor-associated fibroblasts, and CAPZB, forming a bright yellow co-localization signal.

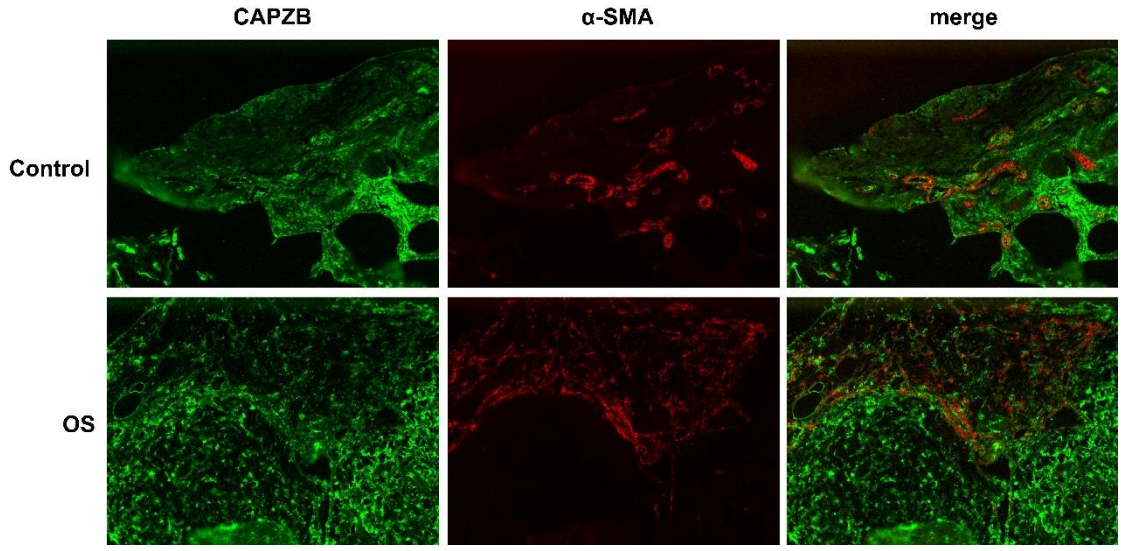

Figure 7. Immunofluorescence depicting the histological localization of CAPZB+CAF-C7 in osteosarcoma and osteoclastoma.

4. Discussion

Over the years, extensive research has been conducted to investigate the regulatory cell death (RCD) pathways that influence tumor formation and development[27-29]. In recent years, there has been a focus on investigating the remodeling of tumor RCD pathways within the tumor microenvironment (TME) to activate pro-inflammatory signals and immunogenicity necessary for anti-tumor immune responses[30]. However, limited attention has been given to exploring the impact of PCD pathways in immunocytes on tumors. In this study, we comprehensively examined the expression of disulfidptosis-related genes in major cell types within the osteosarcoma microenvironment and elucidated the specific associations between disulfidptosis-related subtypes within the TME and osteosarcoma tumors. This unique perspective provides a deeper understanding of how the disulfidptosis pathways of different cellular components within the TME influence the prognosis and outcomes of individual osteosarcoma patients.

Tumor cells constitute the main component of osteosarcoma tissue and play a crucial role in determining patient prognosis and the efficacy of targeted therapies[31]. Additionally, the infiltration of immune cells in osteosarcoma tissue contributes to the complex immune microenvironment that supports the proliferation and invasion of tumor cells[32]. Therefore, it is of great significance to study the major immune cells in the TME and their intricate communication with osteosarcoma cells to develop advanced immunotherapeutic approaches. Notably, lymphocyte infiltration occurs in different regions and subgroups of osteosarcoma, involving multiple molecules with diverse roles in anti-tumor immune responses[33-35]. Tumor-associated macrophages (TAMs) have also garnered attention as potential targets to enhance immunotherapy for osteosarcoma[36]. While clinical trials targeting tumor-associated fibroblasts (CAFs) have had limited success, CAFs remain promising therapeutic targets in cancer treatment[37]. Our study reveals distinct disulfidptosis regulatory patterns in these three components of the tumor microenvironment, highlighting their extensive communication with osteosarcoma cells. Cellchat analysis identified various ligand-receptor pairs, such as LGALS9-CD44, LGALS9-CD45, PTN-NCL, MDK-NCL, MDK-LRP1, SPP1-CD44, MIF-CD74-

 doi:10.20944/preprints202306.1915.v1

CD44, and MIF-CD74-CXCR4, which mediate the communication between disulfidptosis-related subtypes and osteosarcoma cells.

The current tumor-centric treatment approach often fails to eradicate tumors due to metastasis, drug resistance, and the resistant tumor microenvironment[38, 39]. Increasing evidence highlights the critical role of the TME in promoting cancer development, leading researchers to recognize the TME as a key factor in the successful treatment of malignant tumors[40]. Among the diverse stromal components in the TME, CAFs have emerged as major therapeutic targets in various cancer types[41]. To better understand the heterogeneity of CAFs, we classified pan-CAF into five subtypes based on molecular features, including pan-myCAFs, pan-dCAFs, pan-iCAFs, pan-nCAFs, and pan-pCAFs. Specific pan-CAF subtypes have been associated with immune checkpoint blockade (ICB) resistance in different tumors. Our study revealed correlations between distinct disulfidptosis-related fibroblast subtypes and various pan-CAF subtypes. Furthermore, we found that disulfidptosis-related fibroblast subtypes exhibited stronger communication with osteosarcoma cells. Specifically, the CAPZB+CAF subtype showed close associations with pan-myCAF and several pro-inflammatory factors, such as CFD, CFI, C3, C7, CXCL14, CXCL12, among others. Moreover, we identified distinct and specific patterns of cytokine expression among different categories of CAFs. Therefore, we hypothesize that within the osteosarcoma tumor microenvironment, the CAPZB+CAF subtype primarily secretes pro-inflammatory cytokines and plays a crucial role in remodeling the immune microenvironment. Consequently, disulfidptosis-related fibroblast subtypes may mediate the remodeling of the tumor microenvironment and potentially correlate with poor prognosis, tumor growth, and invasion[42-44].

Currently, there is a growing recognition of the pivotal role of programmed cell death (PCD) in the tumor microenvironment (TME)[45]. PCD in certain tumors can elicit immune responses in the TME by releasing cellular components such as pro-inflammatory cytokines and damage-associated molecular patterns[46]. Conversely, PCD in immune cells can directly disrupt anti-tumor immunity within the TME[47, 48]. Therefore, a comprehensive assessment of PCD in different cell types within the TME is crucial for devising effective tumor treatment strategies. In our study, we identified the INF2+Mac subtype through non-negative matrix factorization (NMF) classification, which showed associations with multiple metabolic pathways. Notably, the disulfidptosis-related macrophage subtypes exhibited a closer relationship with metabolism compared to other subtypes. This finding sheds light on the significant role of disulfidptosis in guiding and regulating macrophage metabolism. The metabolic pathways of myeloid cells, represented by macrophages, and lymphocytes, represented by T cells, play pivotal roles in immune activation[49]. Moreover, survival analysis demonstrated a positive impact of the disulfidptosis-related macrophage subtype on overall survival. The INF2+Mac subtype, representing the disulfidptosis-related subtypes, exhibited significant activation of metabolic pathways. The characteristic genes of the INF2+Mac subtype were notably enriched in sulfur metabolism, steroid biosynthesis, starch and sucrose metabolism, oxidative phosphorylation, and other metabolic pathways. Additionally, our study found no significant differences in the distribution of disulfidptosis-related subtypes between M1 and M2 macrophages. Furthermore, we identified extensive associations between four types of infiltrating lymphocytes mediated by disulfidptosis and tumors. Different subtypes exhibited distinct expression patterns of specific cytokines.

To gain further insights into the heterogeneity of gene regulatory networks underlying cellular heterogeneity, we performed transcription factor analysis at the single-cell level. The results revealed distinct transcriptional characteristics among various disulfidptosis-related subtypes, including cancer-associated fibroblasts (CAFs), infiltrating lymphocytes, and macrophages. Several transcription factors, such as JUND, FOS, and IRF1[50-52], were found to be involved in the activation of PCD. However, further research is required to elucidate the specific transcription factors involved in the disulfidptosis process. In summary, similar to other forms of PCD, disulfidptosis-related cell subtypes can regulate different transcription factor networks to reshape the TME. Cell-cell communication analysis using Cellchat unveiled specific interactions between disulfidptosis-related subtypes of various cell populations and osteosarcoma cells. Moreover, within the CAFs subgroup,

disulfidptosis-related subtypes exhibited more extensive cellular communication with osteosarcoma cells, suggesting that the disulfidptosis mode of CAFs may contribute to TME inhibition.

To gain deeper insights into the broader implications of disulfidptosis modes on the tumor microenvironment (TME), we utilized publicly available RNA-seq data to score and evaluate these subtypes in relation to prognosis and response to immunotherapy. The analysis revealed significant prognostic implications of disulfidptosis-related TME subtypes in osteosarcoma, with the subtypes of cancer-associated fibroblasts (CAFs) exhibiting the most pronounced variations in immunotherapy response. These findings were further validated in an independent immunotherapy cohort of bladder cancer (BLCA). Collectively, these results highlight the potential value of disulfidptosis mode in the treatment of osteosarcoma, underscoring its critical significance for subtype investigations within the osteosarcoma TME.

As the first systematic analysis of the impact of disulfidptosis-induced cell death mode in the TME, our conclusions are not without limitations. In addition to the inherent noise and errors in single-cell data, our findings require further validation using a larger clinical sample size. Nevertheless, our study offers a novel perspective on unraveling the characteristics of disulfidptosis-induced cell death in the TME, advancing our understanding of this specific programmed cell death mode, and providing new insights for other domains within the life sciences.

5. Conclusion

We have identified specific disulfidptosis-related subtypes in tumor microenvironment (TME) cells for the first time, using the single-cell sequencing analysis method. Furthermore, we have elucidated the role of intercellular communication mediated by disulfidptosis in the TME, in regulating tumor growth and modulating the anti-tumor immune response. This study provides novel insights into the involvement of disulfidptosis-induced cell death and its impact on the dynamic cellular interactions within the TME, thereby contributing to our understanding of tumor development and immunomodulation

Competing interests The authors declare that they have no competing interests.

Author ContributionsStudy conception and design: Yueying Xiao; Yanqing Huo; Data collection: Yanan Wang; Analysis and interpretation of results: Yueying Xiao; Tianze Zhang; Jin Wang; Draft manuscript preparation: Yueying Xiao; Yanqing Huo; Experiment operation: Yueying Xiao; Revision of the results and approved the final version of the manuscript: Yueying Xiao; Yanqing Huo

Funding This research is funded by the Shengli Oilfield Central Hospital(The contract no:6010220027)

Acknowledgments: We thank The Department of Spine Surgery,The Second Hospital, Shandong University and Key Laboratory of Experimental Teratology of Ministry of Education, Institute of Medical Sciences/Department of Neurology, The Second Hospital, Cheeloo College of Medicine, Shandong University.

Ethics statement: The studies involving human participants were reviewed and approved by Institutional Ethics Committee of the Second Hospital of Shandong University. The patients/participants provided their written informed consent to participate in this study.

Reference

1. Mirabello, L., R.J. Troisi, and S.A. Savage, Osteosarcoma incidence and survival rates from 1973 to 2004: data from the Surveillance, Epidemiology, and End Results Program. Cancer, 2009. 115(7): p. 1531-43.
2. Beird, H.C., et al., Osteosarcoma. Nat Rev Dis Primers, 2022. 8(1): p. 77.
3. Galluzzi, L., et al., Molecular mechanisms of cell death: recommendations of the Nomenclature Committee on Cell Death 2018. Cell Death Differ, 2018. 25(3): p. 486-541.
4. Peng, F., et al., Regulated cell death (RCD) in cancer: key pathways and targeted therapies. Signal Transduct Target Ther, 2022. 7(1): p. 286.
5. Tang, D., et al., Ferroptosis: molecular mechanisms and health implications. Cell Res, 2021. 31(2): p. 107-125.
6. Shin, C.S., et al., The glutamate/cystine xCT antiporter antagonizes glutamine metabolism and reduces nutrient flexibility. Nat Commun, 2017. 8: p. 15074.

7. Koppula, P., et al., The glutamate/cystine antiporter SLC7A11/xCT enhances cancer cell dependency on glucose by exporting glutamate. J Biol Chem, 2017. 292(34): p. 14240-14249.
8. Goji, T., et al., Cystine uptake through the cystine/glutamate antiporter xCT triggers glioblastoma cell death under glucose deprivation. J Biol Chem, 2017. 292(48): p. 19721-19732.
9. Liu, X., et al., Cystine transporter regulation of pentose phosphate pathway dependency and disulfide stress exposes a targetable metabolic vulnerability in cancer. Nat Cell Biol, 2020. 22(4): p. 476-486.
10. Liu, X., et al., Actin cytoskeleton vulnerability to disulfide stress mediates disulfidptosis. Nat Cell Biol, 2023. 25(3): p. 404-414.
11. Xiao, Y. and D. Yu, Tumor microenvironment as a therapeutic target in cancer. Pharmacol Ther, 2021. 221: p. 107753.
12. AlMusawi, S., M. Ahmed, and A.S. Nateri, Understanding cell-cell communication and signaling in the colorectal cancer microenvironment. Clin Transl Med, 2021. 11(2): p. e308.
13. Zhou, Y., et al., Single-cell RNA landscape of intratumoral heterogeneity and immunosuppressive microenvironment in advanced osteosarcoma. Nat Commun, 2020. 11(1): p. 6322.
14. Stine, Z.E., et al., Targeting cancer metabolism in the era of precision oncology. Nat Rev Drug Discov, 2022. 21(2): p. 141-162.
15. Machesky, L.M., Deadly actin collapse by disulfidptosis. Nat Cell Biol, 2023. 25(3): p. 375-376.
16. Satija, R., et al., Spatial reconstruction of single-cell gene expression data. Nat Biotechnol, 2015. 33(5): p. 495-502.
17. Cao, J., et al., The single-cell transcriptional landscape of mammalian organogenesis. Nature, 2019. 566(7745): p. 496-502.
18. Wu, P., et al., A robust semi-supervised NMF model for single cell RNA-seq data. PeerJ, 2020. 8: p. e10091.
19. Jin, S., et al., Inference and analysis of cell-cell communication using CellChat. Nat Commun, 2021. 12(1): p. 1088.
20. Aibar, S., et al., SCENIC: single-cell regulatory network inference and clustering. Nat Methods, 2017. 14(11): p. 1083-1086.
21. Van de Sande, B., et al., A scalable SCENIC workflow for single-cell gene regulatory network analysis. Nat Protoc, 2020. 15(7): p. 2247-2276.
22. Hänzelmann, S., R. Castelo, and J. Guinney, GSVA: gene set variation analysis for microarray and RNA-seq data. BMC Bioinformatics, 2013. 14: p. 7.
23. Jiang, P., et al., Signatures of T cell dysfunction and exclusion predict cancer immunotherapy response. Nat Med, 2018. 24(10): p. 1550-1558.
24. Necchi, A., et al., Atezolizumab in platinum-treated locally advanced or metastatic urothelial carcinoma: post-progression outcomes from the phase II IMvigor210 study. Ann Oncol, 2017. 28(12): p. 3044-3050.
25. Mei, Y., et al., Single-cell characteristics and malignancy regulation of alpha-fetoprotein-producing gastric cancer. Cancer Med, 2023. 12(10): p. 12018-12033.
26. Galbo, P.M., Jr., X. Zang, and D. Zheng, Molecular Features of Cancer-associated Fibroblast Subtypes and their Implication on Cancer Pathogenesis, Prognosis, and Immunotherapy Resistance. Clin Cancer Res, 2021. 27(9): p. 2636-2647.
27. Koren, E. and Y. Fuchs, Modes of Regulated Cell Death in Cancer. Cancer Discov, 2021. 11(2): p. 245-265.
28. Tang, D., et al., The molecular machinery of regulated cell death. Cell Res, 2019. 29(5): p. 347-364.
29. Gao, W., et al., Autophagy, ferroptosis, pyroptosis, and necroptosis in tumor immunotherapy. Signal Transduct Target Ther, 2022. 7(1): p. 196.
30. Tong, X., et al., Targeting cell death pathways for cancer therapy: recent developments in necroptosis, pyroptosis, ferroptosis, and cuproptosis research. J Hematol Oncol, 2022. 15(1): p. 174.
31. Dahlin, D.C. and K.K. Unni, Osteosarcoma of bone and its important recognizable varieties. Am J Surg Pathol, 1977. 1(1): p. 61-72.
32. Wang, H., et al., Subtype Classification and Prognosis Signature Construction of Osteosarcoma Based on Cellular Senescence-Related Genes. J Oncol, 2022. 2022: p. 4421952.
33. Ligon, J.A., et al., Pathways of immune exclusion in metastatic osteosarcoma are associated with inferior patient outcomes. J Immunother Cancer, 2021. 9(5).
34. Sundara, Y.T., et al., Increased PD-L1 and T-cell infiltration in the presence of HLA class I expression in metastatic high-grade osteosarcoma: a rationale for T-cell-based immunotherapy. Cancer Immunol Immunother, 2017. 66(1): p. 119-128.

35. Han, Q., H. Shi, and F. Liu, CD163(+) M2-type tumor-associated macrophage support the suppression of tumor-infiltrating T cells in osteosarcoma. Int Immunopharmacol, 2016. 34: p. 101-106.
36. Tian, H., et al., Managing the immune microenvironment of osteosarcoma: the outlook for osteosarcoma treatment. Bone Res, 2023. 11(1): p. 11.
37. Chen, Y., K.M. McAndrews, and R. Kalluri, Clinical and therapeutic relevance of cancer-associated fibroblasts. Nat Rev Clin Oncol, 2021. 18(12): p. 792-804.
38. Zhou, B.B., et al., Tumour-initiating cells: challenges and opportunities for anticancer drug discovery. Nat Rev Drug Discov, 2009. 8(10): p. 806-23.
39. Kalluri, R., The biology and function of fibroblasts in cancer. Nat Rev Cancer, 2016. 16(9): p. 582-98.
40. Quail, D.F. and J.A. Joyce, Microenvironmental regulation of tumor progression and metastasis. Nat Med, 2013. 19(11): p. 1423-37.
41. Su, S., et al., CD10(+)GPR77(+) Cancer-Associated Fibroblasts Promote Cancer Formation and Chemoresistance by Sustaining Cancer Stemness. Cell, 2018. 172(4): p. 841-856.e16.
42. Sjöberg, E., et al., A Novel ACKR2-Dependent Role of Fibroblast-Derived CXCL14 in Epithelial-to-Mesenchymal Transition and Metastasis of Breast Cancer. Clin Cancer Res, 2019. 25(12): p. 3702-3717.
43. Hornburg, M., et al., Single-cell dissection of cellular components and interactions shaping the tumor immune phenotypes in ovarian cancer. Cancer Cell, 2021. 39(7): p. 928-944.e6.
44. Zeng, M., et al., Manipulation of Transgene Expression in Fibroblast Cells by a Multifunctional Linear-Branched Hybrid Poly(β-Amino Ester) Synthesized through an Oligomer Combination Approach. Nano Lett, 2019. 19(1): p. 381-391.
45. Wu, H.W., et al., The Effects of Programmed Cell Death of Mesenchymal Stem Cells on the Development of Liver Fibrosis. Stem Cells Int, 2023. 2023: p. 4586398.
46. Green, D.R., et al., Immunogenic and tolerogenic cell death. Nat Rev Immunol, 2009. 9(5): p. 353-63.
47. Horton, B.L., et al., Intratumoral CD8(+) T-cell Apoptosis Is a Major Component of T-cell Dysfunction and Impedes Antitumor Immunity. Cancer Immunol Res, 2018. 6(1): p. 14-24.
48. Jarosz-Biej, M., et al., Tumor Microenvironment as A "Game Changer" in Cancer Radiotherapy. Int J Mol Sci, 2019. 20(13).
49. Jung, J., H. Zeng, and T. Horng, Metabolism as a guiding force for immunity. Nat Cell Biol, 2019. 21(1): p. 85-93.
50. Lei, S., et al., JUND/linc00976 promotes cholangiocarcinoma progression and metastasis, inhibits ferroptosis by regulating the miR-3202/GPX4 axis. Cell Death Dis, 2022. 13(11): p. 967.
51. Liu, Z., et al., PCDH7 knockdown potentiates colon cancer cells to chemotherapy via inducing ferroptosis and changes in autophagy through restraining MEK1/2/ERK/c-Fos axis. Biochem Cell Biol, 2022. 100(6): p. 445-457.
52. Zhang, Y., et al., IRF1/ZNF350/GPX4-mediated ferroptosis of renal tubular epithelial cells promote chronic renal allograft interstitial fibrosis. Free Radic Biol Med, 2022. 193(Pt 2): p. 579-594.

Figures

Figure 1: Overview of the study on disulfidptosis-related genes in osteosarcoma single-cell data. (A) Expression of 14 disulfidptosis-related genes depicted on a t-SNE plot. (B) UMAP visualization showing 11 cell types within the single-cell clusters. (C) Cellchat analysis illustrating intercellular communication among the 11 major cell types. (D) Heatmap displaying the distribution of disulfidptosis-related genes in various cell types, including osteoblastic OS cells, proliferating osteoblastic OS cells, chondroblastic OS cells, osteoclastic cells, TILs (T and NK cells), myeloid cells, fibroblasts, pericytes, MSCs, myoblasts, and endothelial cells. (E) Violin plots presenting the expression of four genes closely associated with disulfidptosis regulation.

Figure 2: Impact of disulfidptosis on fibroblast characteristics. (A) Cell communication between disulfidptosis-related fibroblast subtypes and osteosarcoma cells. (B) Cell communication between different disulfidptosis-related subtypes, indicating the weightage of each interaction. (C) Association of different disulfidptosis-related subtypes with five pan-CAF subtypes. (D) Pseudotime analysis depicting a clustered heatmap of 14 disulfidptosis-related genes in fibroblasts. (E) Incoming and outgoing signaling patterns of disulfidptosis-related fibroblast subtypes. (F) Comparison of transcription factor activities in seven disulfidptosis-related fibroblast subtypes using the SCENIC

package in R. (G) Heatmap displaying the average expression of seven common signaling pathway genes across different disulfidptosis-related fibroblast subtypes.

Figure 3: NMF clusters of disulfidptosis-related genes for tumor-infiltrating lymphocytes. (A) UMAP and tSNE maps illustrating the cellular distribution of eight infiltrating lymphocyte subpopulations, including CD4+T cells, B cells, CD8+T cells, natural killer (NK) cells, CD4-/CD8- T cells, proliferating T cells, NKT cells, and regulatory T cells (T-reg). (B) Heatmap displaying different features of NMF clusters, such as four T cell functional scores and the average expression of immune inhibitory and immune activation genes in the four infiltrating lymphocyte subtypes. (C) Cell-cell communication between disulfidptosis-related infiltrating lymphocytes and osteosarcoma cells. (D) Comparison of transcription factor activities in the four infiltrating lymphocyte subtypes using the SCENIC package in R.

Figure 4: Impact of disulfidptosis on macrophage characteristics. (A) Cell communication between disulfidptosis-related macrophage subtypes and osteosarcoma cells. (B) t-SNE plot of myeloid cells in osteosarcoma TME; UMAP plot of different disulfidptosis-related macrophage subtypes. (C) Pseudotime analysis depicting a clustered heatmap of 14 disulfidptosis-related genes in macrophages. (D) Incoming and outgoing signaling patterns of disulfidptosis-related macrophage subtypes. (E) Heatmap illustrating the scoring differences of four disulfidptosis-related macrophage subtypes across 30 metabolic signaling pathways. (F) UMAP plots of M1 macrophages and M2 macrophages. (G) Differential expression of disulfidptosis-related subtypes in M1 macrophages and M2 macrophages. (H) Cellular trajectories of different disulfidptosis-related subtypes using monocle.

Figure 5: Prognosis and immunotherapy response of disulfidptosis-related subtypes (GSVA scores) in different public cohorts. (A) Analysis of immunotherapy response. (B) Prognosis analysis. (C) Immunotherapy response in a public cohort.

Figure 6: Intercellular communication between major disulfidptosis-related subtypes. (A) Ligand-receptor interactions between major disulfidptosis-related subtypes and osteosarcoma. (B) Cellchat analysis demonstrating cell-cell communication among disulfidptosis-related subtypes.

Figure 7: Immunofluorescence depicting the histological localization of CAPZB+CAF-C7 in osteosarcoma and osteoclastoma.

Supplementary Figure 1: Communication analysis and features of disulfidptosis-related subtypes in CD8+ T cells. (A) Cell-cell communication between disulfidptosis-related CD8+ T subtypes and osteosarcoma cells. (B) Pseudotime analysis displaying a clustered heatmap of 14 disulfidptosis-related genes in CD8+ T cells. (C) Incoming and outgoing signaling patterns of disulfidptosis-related CD8+ T subtypes. (D) UMAP plots illustrating different disulfidptosis-related CD8+ T subtypes. (E) Cellular trajectories of different disulfidptosis-related CD8+ T subtypes using monocle.

Supplementary Figure 2: Communication analysis and features of disulfidptosis-related subtypes in CD4+ T cells. (A) Cell-cell communication between disulfidptosis-related CD4+ T subtypes and osteosarcoma cells. (B) Pseudotime analysis depicting a clustered heatmap of 14 disulfidptosis-related genes in CD4+ T cells. (C) Incoming and outgoing signaling patterns of disulfidptosis-related CD4+ T subtypes. (D) UMAP plots demonstrating different disulfidptosis-related CD4+ T subtypes. (E) Cellular trajectories of different disulfidptosis-related CD4+ T subtypes using monocle.

Supplementary Figure 3: Communication analysis and features of disulfidptosis-related subtypes in NK cells. (A) Cell-cell communication between disulfidptosis-related NK cell subtypes and osteosarcoma cells. (B) Pseudotime analysis presenting a clustered heatmap of 14 disulfidptosis-related genes in NK cells. (C) Incoming and outgoing signaling patterns of disulfidptosis-related NK cell subtypes. (D) UMAP plots illustrating different disulfidptosis-related NK cell subtypes. (E) Cellular trajectories of different disulfidptosis-related NK cell subtypes using monocle.

Supplementary Figure 4: Communication analysis and features of disulfidptosis-related subtypes in regulatory T cells. (A) Cell-cell communication between disulfidptosis-related regulatory T cell subtypes and osteosarcoma cells. (B) Pseudotime analysis presenting a clustered heatmap of 14 disulfidptosis-related genes in regulatory T cells. (C) Incoming and outgoing signaling patterns of disulfidptosis-related regulatory T cell subtypes. (D) UMAP plots demonstrating different

 doi:10.20944/preprints202306.1915.v1

disulfidptosis-related regulatory T cell subtypes. (E) Cellular trajectories of different disulfidptosis-related regulatory T cell subtypes using monocle.

Supplementary Figure 5: Prognosis of disulfidptosis-related subtypes (GSVA scores) in different public cohorts.

Supplementary Figure 6: Immunotherapy response of disulfidptosis-related subtypes (GSVA scores) in different public cohorts.

Supplementary Figure 7: Ligand-receptor interactions between all disulfidptosis-related subtypes and osteosarcoma cells.

Additional Files

Supplementary Table1.xls: Marker genes for all disulfidptosis-related subtypes.

Supplementary Table2.xls: T-cell signature genes.